Optical performance and metallic absorption in nanoplasmonic systems

Matthew D. Arnold* **and Martin G. Blaber**

Institute for Nanoscale Technology, Department of Physics and Applied Materials, University of Technology Sydney, PO Box 123 Broadway, NSW 2007, Australia

**Corresponding author: Matthew.Arnold-1@uts.edu.au*

Abstract: Optical metrics relating to metallic absorption in representative plasmonic systems are surveyed, with a view to developing heuristics for optimizing performance over a range of applications. We use the real part of the permittivity as the independent variable; consider strengths of particle resonances, resolving power of planar lenses, and guiding lengths of planar waveguides; and compare nearly-free-electron metals including Al, Cu, Ag, Au, Li, Na, and K. Whilst the imaginary part of metal permittivity has a strong damping effect, field distribution is equally important and thus factors including geometry, real permittivity and frequency must be considered when selecting a metal. Al performs well at low permittivities (e.g. sphere resonances, superlenses) whereas Au & Ag only perform well at very negative permittivities (shell and rod resonances, LRSPP). The alkali metals perform well overall but present engineering challenges.

OCIS codes: (250.5403) Plasmonics; (160.3900) Metals; (310.6628) Subwavelength structures.

References and links

1. E. Ozbay, "Plasmonics: Merging photonics and electronics at nanoscale dimensions," Science **311**, 189-193 (2006).
2. D. Pissuwan, S. M. Valenzuela, and M. B. Cortie, "Therapeutic possibilities of plasmonically heated gold nanoparticles," Trends Biotechnol. **24**, 62-67 (2006).
3. D. Pissuwan, S. M. Valenzuela, C. M. Miller, and M. B. Cortie, "A Golden Bullet? Selective Targeting of Toxoplasma gondii Tachyzoites Using Antibody-Functionalized Gold Nanorods," Nano. Lett. **7**, 3808-3812 (2007).
4. N. Engheta, A. Salandrino, and A. Alu, "Circuit Elements at Optical Frequencies: Nanoinductors, Nanocapacitors, and Nanoresistors," Phys. Rev. Lett. **95**, 095504-095504 (2005).
5. N. Engheta, "Circuits with Light at Nanoscales: Optical Nanocircuits Inspired by Metamaterials," Science **317**, 1698-1702 (2007).
6. Z. W. Liu, S. Durant, H. Lee, Y. Pikus, N. Fang, Y. Xiong, C. Sun, and X. Zhang, "Far-field optical superlens," Nano. Lett. **7**, 403-408 (2007).
7. U. Kreibig and M. Vollmer, *Optical properties of metal clusters* (Springer-Verlag, Berlin Heidelberg, 1995).
8. H. Raether, *Surface Plasmons on Smooth and Rough Surfaces and on Gratings*, Springer Tracts in Modern Physics (Springer, 1988).
9. M. Kuttge, E. J. R. Vesseur, J. Verhoeven, H. J. Lezec, H. A. Atwater, and A. Polman, "Loss mechanisms of surface plasmon polaritons on gold probed by cathodoluminescence imaging spectroscopy," Appl. Phys. Lett. **93**, 113110-113113 (2008).
10. M. G. Blaber, M. D. Arnold, and M. J. Ford, "Optical properties of intermetallic compounds from first principles: a search for the ideal plasmonic material," J. Phys. Condens. Matter (2009).
11. J. H. Weaver and H. P. R. Frederikse, *Optical properties of selected elements 82 ed.* (CRC Press, Boca Raton, FL, 2001).
12. T. Hagihara, Y. Hayashiuchi, and T. Okada, "Photoplastic effects in colored KCl single crystals containing potassium metal colloids. I. Preparation of specimens enriched with potassium metal colloids," Osaka Kyoiku Daigaku Kiyo, Dai-3-bumon: Shizen Kagaku, Oyo Kagaku **46**, 49-56 (1997).
13. C. F. Bohren and D. R. Huffman, *Absorption and scattering of light by small particles* (Wiley, Weinheim, 2004).

#106659 - $15.00 USD Received 21 Jan 2009; revised 23 Feb 2009; accepted 24 Feb 2009; published 26 Feb 2009

14. E. Hao and G. C. Schatz, "Electromagnetic fields around silver nanoparticles and dimers," J. Chem. Phys. **120**, 357-366 (2004).
15. M. Blaber, N. Harris, M. J. Ford, and M. B. Cortie, "Optimisation of absorption efficiency for varying dielectric spherical nanoparticles," in *International Conference on Nanoscience and Nanotechnology, 2006. ICONN '06.*, 2006),
16. M. G. Blaber, M. D. Arnold, N. Harris, M. J. Ford, and M. B. Cortie, "Plasmon absorption in nanospheres: A comparison of sodium, potassium, aluminium, silver and gold," Physica B **394**, 184-187 (2007).
17. F. Wang and Y. R. Shen, "General Properties of Local Plasmons in Metal Nanostructures," Phys. Rev. Lett. **97**, 206806-206804 (2006).
18. U. Evra and D. J. Bergman, "Lifetime of nanoplasmonic states," in *Plasmonics: Nanoimaging, Nanofabrication, and their Applications II*, (SPIE, 2006), 63240H-63212.
19. E. Prodan, C. Radloff, N. J. Halas, and P. Nordlander, "A hybridization model for the plasmon response of complex nanostructures," Science **302**, 419-422 (2003).
20. N. Harris, M. J. Ford, P. Mulvaney, and M. B. Cortie, "Tunable infrared absorption by metal nanoparticles: The case for gold rods and shells," Gold Bulletin **41**, 5-14 (2008).
21. S. W. Prescott and P. Mulvaney, "Gold nanorod extinction spectra," J. Appl. Phys. **99**, 123504-123507 (2006).
22. G. W. Bryant, I. Romero, F. J. G. de Abajo, and J. Aizpurua, "Simulating electromagnetic response in coupled metallic nanoparticles for nanoscale optical microscopy and spectroscopy: nanorod-end effects," in *Plasmonics: Metallic Nanostructures and their Optical Properties IV*, (SPIE, 2006), 632313-632318.
23. S. Asano and G. Yamamoto, "Light-Scattering by a Spheroidal Particle," Appl. Opt. **14**, 29-49 (1975).
24. R. Gans, "Ãœber die Form ultramikroskopischer Goldteilchen," Annalen der Physik **342**, 881-900 (1912).
25. J. B. Pendry, "Negative refraction makes a perfect lens," Phys. Rev. Lett. **85**, 3966-3969 (2000).
26. V. M. Shalaev, "Optical negative-index metamaterials," Nature Photon. **1**, 41-48 (2007).
27. R. A. Shelby, D. R. Smith, and S. Schultz, "Experimental verification of a negative index of refraction," Science **292**, 77-79 (2001).
28. J. Valentine, S. Zhang, T. Zentgraf, E. Ulin-Avila, D. A. Genov, G. Bartal, and X. Zhang, "Three-dimensional optical metamaterial with a negative refractive index," Nature **455**, 379 (2008).
29. Z. W. Liu, H. Lee, Y. Xiong, C. Sun, and X. Zhang, "Far-field optical hyperlens magnifying sub-diffraction-limited objects," Science **315**, 1686-1686 (2007).
30. Z. Jacob, L. V. Alekseyev, and E. Narimanov, "Optical hyperlens: Far-field imaging beyond the diffraction limit," Opt. Express **14**, 8247-8256 (2006).
31. K. Li, M. I. Stockman, and D. J. Bergman, "Self-Similar Chain of Metal Nanospheres as an Efficient Nanolens," Phys. Rev. Lett. **91**, 227402 (2003).
32. M. D. Arnold and R. J. Blaikie, "Subwavelength optical imaging of evanescent fields using reflections from plasmonic slabs," Opt. Express **15**, 11542-11552 (2007).
33. S. A. Ramakrishna and J. B. Pendry, "The asymmetric lossy near-perfect lens," J. Mod Opt. **49**, 1747-1762 (2002).
34. D. O. S. Melville and R. J. Blaikie, "Super-resolution imaging through a planar silver layer," Opt. Express **13**, 2127-2134 (2005).
35. S. A. Ramakrishna, J. B. Pendry, M. C. K. Wiltshire, and W. J. Stewart, "Imaging the near field," J. Mod Opt. **50**, 1419-1430 (2003).
36. S. A. Ramakrishna, "Physics of negative refractive index materials," Rep. Prog. Phys. **68**, 449-521 (2005).
37. D. O. S. Melville and R. J. Blaikie, "Experimental comparison of resolution and pattern fidelity in single- and double-layer planar lens lithography," J. Opt. Soc. Am. B **23**, 461-467 (2006).
38. C. P. Moore, M. D. Arnold, P. J. Bones, and R. J. Blaikie, "Image fidelity for single-layer and multi-layer silver superlenses," J. Opt. Soc. Am. A **25**, 911-918 (2008).
39. P. Berini, "Figures of merit for surface plasmon waveguides," Opt. Express **14**, 13030-13042 (2006).
40. R. Buckley and P. Berini, "Figures of merit for 2D surface plasmon waveguides and application to metal stripes," Opt. Express **15**, 12174-12182 (2007).
41. W. L. Barnes, "Surface plasmon–polariton length scales: a route to sub-wavelength optics," J. Opt. A **8**, S87–S93 (2006).
42. R. Zia, M. D. Selker, P. B. Catrysse, and M. L. Brongersma, "Geometries and materials for subwavelength surface plasmon modes," J. Opt. Soc. Am. A **21**, 2442-2446 (2004).
43. R. Ruppin, "Electromagnetic energy density in a dispersive and absorptive material," Phys. Lett. A **299**, 309-312 (2002).
44. S. I. Bozhevolnyi and T. Søndergaard, "General properties of slow-plasmon resonant nanostructures: nano-antennas and resonators," Opt. Express **15**, 10869-10877 (2007).
45. S. A. Maier, *Plasmonics. Fundamentals and Applications* (Springer, New York, 2007).
46. M. Fukui, T. Okamoto, T. Ogawa, M. Haraguchi, D. F. P. Pile, and D. K. Gramotnev, "Characteristics of plasmonic waveguides and nonlinear metallic particles," in *Plasmonics: Nanoimaging, Nanofabrication, and their Applications II*, (SPIE, 2006), 632401-632410.

#106659 - $15.00 USD Received 21 Jan 2009; revised 23 Feb 2009; accepted 24 Feb 2009; published 26 Feb 2009

47. E. N. Economou, "Surface Plasmons in Thin Films," Phys. Rev. **182**, 539 (1969).

1. Introduction

Plasmonics is an active area of research [1], due to the potential for high performance in areas such as medical diagnostics [2] and therapeutics [3], communications [4], computing [5], and imaging [6]. One of the limiting factors in all plasmonics is loss, which arises due to many processes, including radiative damping, electron confinement, structural imperfections, and metal heating losses. Our primary focus here is the bulk-metal properties; nonetheless all these loss processes can be important in various regimes. Radiative damping [7] can usually be minimized by keeping geometries small, but not so small that electron confinement and surface scattering dominate [7]. Structural imperfections including surface roughness [8] and grain boundaries [9] are essentially a technical process issue affecting optical properties and cannot be easily predicted. Methods for summing the various damping contributions are available [7], so it is plausible to consider heating losses separately. The key question we consider here is what permittivity profile actually constitutes a good plasmonic material?

We will consider only non-magnetic metals with permittivity $\varepsilon = \varepsilon_0(\varepsilon' + i\varepsilon'')$. The frequency dependence is of considerable practical importance, but fundamentally we are interested in the relationship between real and imaginary permittivity, and we will show later that ε' describes the operating point of plasmonic systems and ε'' describes loss. Metallic loss is induced by two key processes: interband and intraband transitions. Good metals have comparatively weak interband transitions that are not easy to predict [10], so we consider this effect only in the context of measured permittivity values. Conversely, intraband transitions are fundamental to metals and are reasonably captured by the Drude model [7], and by eliminating frequency ω this can be written:

$$\varepsilon'' = \left[\frac{(1-\varepsilon')^3}{(\gamma/\omega_p)^{-2} - (1-\varepsilon')} \right]^{1/2} \tag{1}$$

where γ is the damping frequency and ω_p is the plasma frequency. The ratio γ/ω_p describes the strength of the intraband damping, which for many real metals lies in the range 10^{-3} to 10^{-2} as demonstrated in Fig. 1. The form of the permittivity functional (1) varies widely depending on ε' but we will focus on the region $-(\gamma/\omega_p)^{-2} < \varepsilon' < -1$, where $\varepsilon'' << |\varepsilon'|$ suggesting damping is comparatively small. In this region, the low loss limit of the frequency-dependent Drude model suggests a fundamental scaling $\omega \sim \omega_p\sqrt{-\varepsilon'}$, which could in theory be used to eliminate frequency from later relationships, but this has very limited applicability especially in the context of real metals.

Real metals can differ significantly from the Drude model especially at smaller permittivities, so measured permittivity values are needed. Here, we use the experimentally determined optical functions of Weaver and Frederikse [11], although it is worth noting that reported properties vary significantly depending on preparation and measurement techniques. For clarity we will not present any other data here, and limit our results to the best performing metals from [11], including Cu due to its important role in the development of metamaterials. Alkali metals are also included for their excellent optical properties – obviously their chemical characteristics are less than desirable, nevertheless some alkali plasmonic systems have been constructed [12].

#106659 - $15.00 USD Received 21 Jan 2009; revised 23 Feb 2009; accepted 24 Feb 2009; published 26 Feb 2009

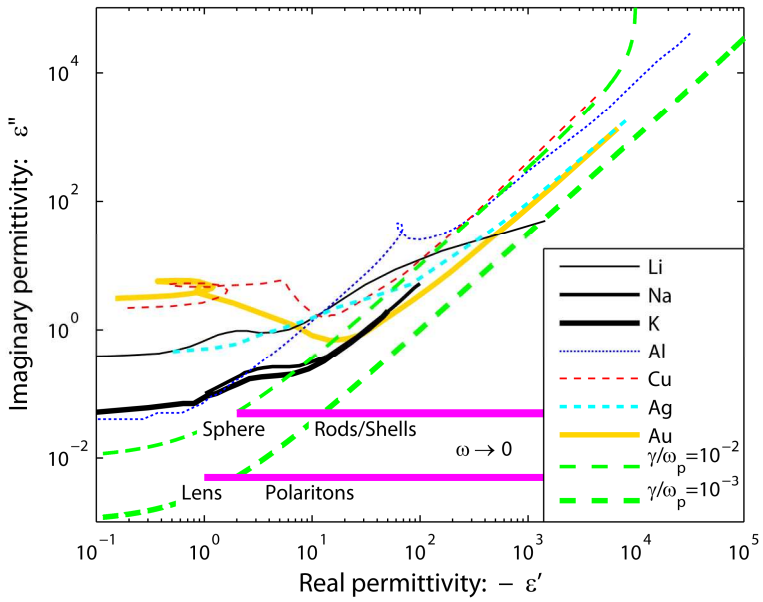

Fig. 1. Permittivity functional for the chosen metals and two Drude models for comparison. Example plasmonic systems are overlaid, showing the real part of permittivity required for operation.

The effect of ε'' can be considered in the context of the energy balance of the system, because energy is extracted by metal absorption at a rate given by:

$$\left\langle \dot{U} \right\rangle = \int_{metal} \frac{1}{2} \omega \varepsilon_0 \varepsilon'' \left| E \right|^2 dV \tag{2}$$

This implies low ε'' can decrease absorption, but note also that absorption depends strongly on the electric field distribution $|\mathrm{E}|$. This is an important point because good plasmonic performance is often associated with resonances, resulting in strong fields and therefore high absorption. The extent to which field distribution relates to performance may differ between systems, and thus the relationship between ε'' and performance must be considered on a case-by-case basis.

Importantly, ε'' affects field strength, but so does ε', and we can optimize performance through this by changing geometry and background permittivity. We assert that the best independent variable for comparison is the real part of the metal permittivity ε'. For all the systems we consider, ε' determines the operating point of the system (as a ratio with the background medium ε_b), whereas the frequency ω is only coincidentally related. Specific examples of this include the flat plasmonic lens (ratio -1) and dipole sphere resonance (ratio -2). A wider range of ratios is possible with general systems involving surface-plasmon-polaritons (SPPs) and particularly localized surface plasmons (LSPs), ranging from zero (high frequency) to large negative ratios (low frequency). Once a usable range of ε' is identified, it is then simple to choose geometric factors to achieve optimal performance. With that in mind we now examine performance metrics associated with some representative systems and attempt to infer general scalings from these. Systems to be considered include nanoparticle resonances, planar plasmonic lenses and planar SPP waveguides.

#106659 - $15.00 USD Received 21 Jan 2009; revised 23 Feb 2009; accepted 24 Feb 2009; published 26 Feb 2009

2. Nanoparticle resonances

Metal nanoparticles have strong resonances associated with LSPs [13]. The literature has numerous examples of optimizations for specific particles [14], and specific metals, most often gold or silver, have been studied widely. Only a few broad material surveys have been performed for sphere absorption [15, 16], and few or none consider a wide range of metrics. Small particles are dominated by the electric dipole resonance, which can be described via the geometry, volume, and permittivity dependent polarizability α . This can be easily related [13] to the pertinent metrics: absorption, scattering and field enhancement.

Before considering the polarizability for various geometries, it is first instructive to consider resonances in a more general sense [17], [18]. The assumptions used are low-loss metals and small particles (low scattering), and the general approach is to consider energy processes. The particles should not be too small that surface scattering becomes appreciable. The resonance quality factor, a dimensionless metric for absorptive damping which is geometry independent is then [17]:

$$Q \equiv \frac{\omega}{\Delta\omega} = \frac{\omega\langle U\rangle}{\langle \dot{U}\rangle} \approx \frac{\omega}{2\varepsilon''}\frac{d\varepsilon'}{d\omega} \tag{3}$$

Figure 2 shows a plot of this quality factor for a range of metallic elements.

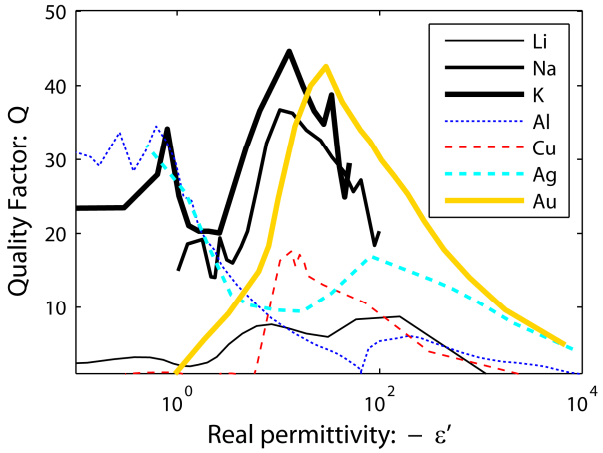

Fig. 2. Nanoparticle resonance quality factor for various metals. Note that since Q is independent of background permittivity, compensation for background requires only proportional scaling of the independent variable.

Figure 2 gives an overview of the discussion that follows, remembering that the specific conclusions drawn rely on a particular dataset. It is clear that some metals perform best at low permittivities (especially Al), others perform better at high permittivities (especially Au), and that K is generally the best overall. This allows optimization by showing the best metal-permittivity pairs, which could then be matched to geometric factors according to the particular situation, as noted on Fig. 1.

2.1 Spherical core-shell resonances

Returning now to the dipole strength of particular geometries, we first consider a spherical metal shell coating a spherical dielectric core of permittivity ε_c . This geometry is relatively easy to model and has been extensively studied. It is well known that "hybridization" of dipole sphere $\varepsilon' = -2\varepsilon_b$ and cavity modes $\varepsilon' = -\varepsilon_b / 2$ leads to red- and blue- shifted modes,

#106659 - $15.00 USD Received 21 Jan 2009; revised 23 Feb 2009; accepted 24 Feb 2009; published 26 Feb 2009

with the higher order modes lying in between [19]. We are most interested in the red-shifted dipole mode since it typically dominates, and the real metals studied here generally perform better at longer wavelengths. As usual most optimizations of the general case have considered silver and gold where thin shells perform better [20], but this may not necessarily hold for more Drude-like metals. The known expression [13] for α can be manipulated to find the value at resonance for $\varepsilon'' \to 0$, and we approximate the result again for $\varepsilon'' \to 0$ to give the approximate *resonance* strength for the optimum shell geometry:

$$\alpha \approx iV \frac{9\varepsilon_b \varepsilon'(-\varepsilon' + \varepsilon_c)(2\varepsilon' + \varepsilon_c)}{2\varepsilon''(\varepsilon_c + 2\varepsilon_b)([\varepsilon']^2 - \varepsilon_c \varepsilon_b)} \tag{4}$$

Strictly this expansion for peak α is invalid at very low frequencies, because then ε'' could be greater than ε_b, ε_c and ε', resulting in potentially inaccurate field enhancements. However, the cross-sections remain usable due to the scaling effect of frequency. Importantly, there are no dipole modes in the range $-2\varepsilon_b < \varepsilon' < -\varepsilon_c / 2$ and the approximation is invalid in that region. The dipole resonance strength derived in Eq. (4) for a range of elemental metals is plotted in Fig. 3 and the peak strengths are compared in Table 1.

The results again show that Al only performs well at low permittivities, Au has an optimum at larger permittivity, and K is the best overall. These trends are reflected in the specific optima listed in Table 1 – a solid sphere is the best for Al because of its poor performance at high permittivities, whereas for Au a thin shell about 5% of the outer radius is required to red-shift the resonance to the best permittivity, however such thin shells may result in additional damping due to surface scattering. The peak dipole of K is about 20% stronger than Au.

To clarify the behaviour of Eq. (4), we derive the limiting cases of very negative permittivity (red-shifted modes), and weak permittivity, respectively:

$$\alpha \to -iV \frac{9\varepsilon_b \varepsilon'}{(\varepsilon_c + 2\varepsilon_b)\varepsilon''} \text{ when } |\varepsilon'| >> \varepsilon_b, \varepsilon_c \tag{5}$$

$$\alpha \to -iV \frac{9\varepsilon_c \varepsilon'}{2(\varepsilon_c + 2\varepsilon_b)\varepsilon''} \text{ when } |\varepsilon'| << \varepsilon_b, \varepsilon_c \tag{6}$$

Red-shifted resonances are well described by Eq. (5), but few real metals (except Al) are accurately represented by Eq. (6) as interband transitions dominate in this regime, resulting in $\varepsilon'' > |\varepsilon'|$. The sphere and cavity mode strengths are given by $\alpha \approx iV 9\varepsilon_b / (2\varepsilon'') = iV 9\varepsilon' / \varepsilon''$ and $\alpha \to 0$ respectively.

Note that for symmetric dielectrics ($\varepsilon_b = \varepsilon_c$), the polarizability is mostly independent of that environment. In a non-symmetric environment, the low-frequency mode is most strongly influenced by the core permittivity: as core permittivity goes up, dipole strength is reduced. In other respects the data shown does not qualitatively change, except that the relative shell thickness required to match a given metal permittivity is increased, and conversely the permittivity cut-off for this type of mode becomes more negative.

#106659 - $15.00 USD Received 21 Jan 2009; revised 23 Feb 2009; accepted 24 Feb 2009; published 26 Feb 2009

Table 1. of peak dipole strengths for spherical shells in vacuum, with required parameters.

Metal	$\lvert\alpha\rvert/V$	λ (μm)	$-\varepsilon'$	core volume fraction
Li	>87	>8.86	>1444	>0.997
Na	111	0.87	14.2	0.72
K	126	1.12	11.5	0.67
Al	55	0.14	2	0
Cu	31	0.71	18.4	0.78
Ag	50	1.44	112	0.96
Au	105	0.91	32	0.87

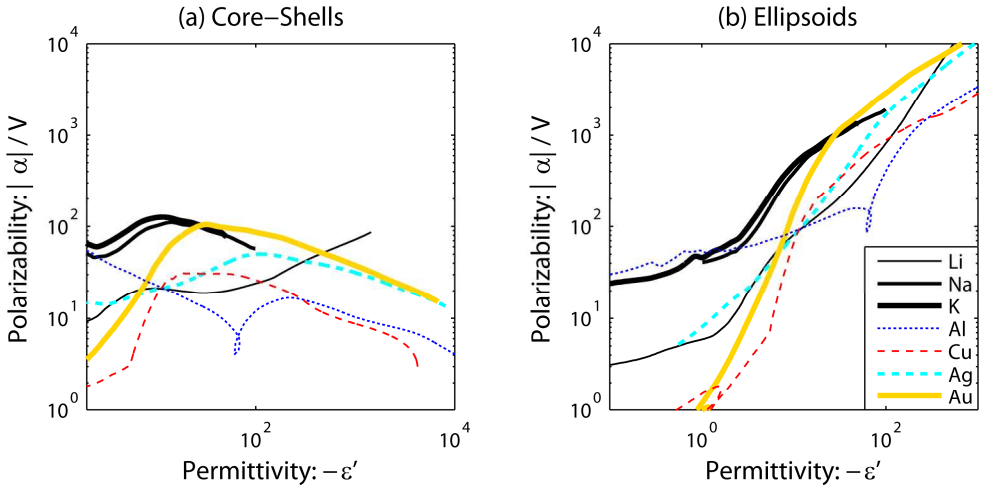

Fig. 3. Approximate dipole strength of low-frequency core-shell modes (left, from Eq. 4), and ellipsoids (right, Eq. 7) embedded in vacuum. The approximation is accurate in the region shown, except for Cu at small permittivities.

2.2 Ellipsoid resonances

We also consider solid ellipsoids, which may be solved analytically and serve as convenient substitute for the geometrically related nanorods. Nanorods have been studied extensively due to strong absorption [20], and it is known that the precise shape of the rod has some bearing on the optical performance [21] [22], however the general case can only be solved numerically. The fully-retarded solution for an ellipsoid is quite complicated [23], but small particles can be adequately described by the dipole approximation [13]. Once again we derive the low-loss case $\varepsilon'' \to 0$ for the optimum ellipsoid anisotropy:

$$\alpha \approx iV \frac{(\varepsilon' - \varepsilon_b)^2}{\varepsilon'' \varepsilon_b} \tag{7}$$

#106659 - $15.00 USD Received 21 Jan 2009; revised 23 Feb 2009; accepted 24 Feb 2009; published 26 Feb 2009

Note the stronger influence of ε' on the ellipsoid compared to the spherical shell (Eq. 4), presumably due to the larger field deformation required to achieve boundary matching in the anisotropic coordinates.

This expression does not discriminate between the different resonances exhibited by ellipsoids. There are at most three unique resonances, one for each axis, and it is easier to understand uniaxial ellipsoids (spheroids) that have only two. Prolate spheroids, $r_a > r_b = r_c$ (rods) have a longitudinal resonance ($\varepsilon' \to -\infty$) and a doubly-degenerate transverse resonance ($\varepsilon' \to -\varepsilon_b$), whereas oblate spheroids, $r_a < r_b = r_c$ (disks) have a doubly-degenerate disk resonance ($\varepsilon' \to -\infty$) and a bulk-like film resonance ($\varepsilon' \to 0$) [24]. The simplest special case is a sphere which has only one triply-degenerate resonance. Considering these special cases, we find the following:

longitudinal prolate mode and oblate disk modes,

$$\alpha \to iV \frac{[\varepsilon']^2}{\varepsilon'' \varepsilon_b} \text{ when } |\varepsilon'| >> \varepsilon_b , \tag{8}$$

transverse prolate ellipsoid modes,

$$\alpha \approx iV \frac{4\varepsilon_b}{\varepsilon''} = -iV \frac{4\varepsilon'}{\varepsilon''} \text{ when } \varepsilon' = -\varepsilon_b , \tag{9}$$

and oblate film resonance,

$$\alpha \to iV \frac{\varepsilon_b}{\varepsilon''} \text{ when } |\varepsilon'| << \varepsilon_b . \tag{10}$$

These expressions predict that high background permittivity increases dipole strength at low metal permittivities (high frequencies) and vice-versa. Additionally the relationship between metal permittivity and aspect ratio is scaled – a given metal permittivity requires a less anisotropic ellipsoid.

Dipole strengths for metal ellipsoids according to Eq. (8) are plotted in Fig. 3(b). The results show that dipole strength is maximum at large negative permittivities, corresponding to highly anisotropic ellipsoids and low frequencies. Na and K perform well overall, whereas Li, Au and Ag perform better at low frequencies. Al is the best metal at low permittivities, but due to the weakness of ellipsoids at low permittivities it is not ideal overall.

3. Plasmonic lensing

Plasmonic lenses have negative permittivity which allows super-resolution of near-field objects [25]. Better flexibility can be achieved with metamaterials that have negative refractive index [26, 27]. Despite the difficulties involved in implementing the required resonator arrays for use in the optical regime, there have been some impressive developments [28]. Although similar arguments link lens optical properties to resolving power for both negative permittivity and negative refractive index materials, the derivation of metrics for metamaterials is heavily system dependent and lies outside the scope of the present work. Several geometries have been reported for negative permittivity superlenses [29-32], but we will focus on planar lenses [33] since these have been the most extensively studied and implemented [34].

The planar superlensing condition in a symmetric environment is given by $\varepsilon' = -\varepsilon_b$, with equal thicknesses d of dielectric and metal. Resolution is determined by examining the spatial dispersion of thin film transmission t from object-to-image, and sufficient strength of

#106659 - $15.00 USD Received 21 Jan 2009; revised 23 Feb 2009; accepted 24 Feb 2009; published 26 Feb 2009

evanescent waves with transverse wavevector $k_t > \sqrt{\varepsilon_b}\omega/c$ is required for super-resolution. Strictly, evanescent waves do not transfer energy to the image unless there is a perturbation such as a weakly absorbing photosensitive layer that could extract energy from the electric field. The actual imaging performance depends on how the energy is extracted, but $|t|$ gives some indication. An approximate expression for the resolution Δ of a single layer lens has been derived by determining a corner or "cutoff" wavevector $k_{\max}$ [35]:

$$\frac{1}{\Delta} = \frac{k_{\max}}{2\pi} \sim -\frac{1}{2\pi d} \ln\left[-\frac{\varepsilon''}{2\varepsilon'}\right] \tag{11}$$

Similarly, and applying the effective medium limit, the multilayer lens result is [35]:

$$\frac{1}{\Delta} \sim -\frac{\varepsilon'}{2\pi d \varepsilon''} \tag{12}$$

Several studies [16, 36] have used "resolution enhancement" λ/Δ, however wavelength does not affect evanescent propagation and we instead plot the other dimensionless ratio d/Δ. It is important to keep in mind that all evanescent imaging techniques are constrained in the sense that the depth-of-field for the image is proportional to Δ. Also, for this particular geometry the sum of object-to-metal and metal-to-image distance is only d/N where N is the number of layers, and object-to-image distance is $2d$. Equation (11) and Eq. (12) are plotted in Fig. 4.

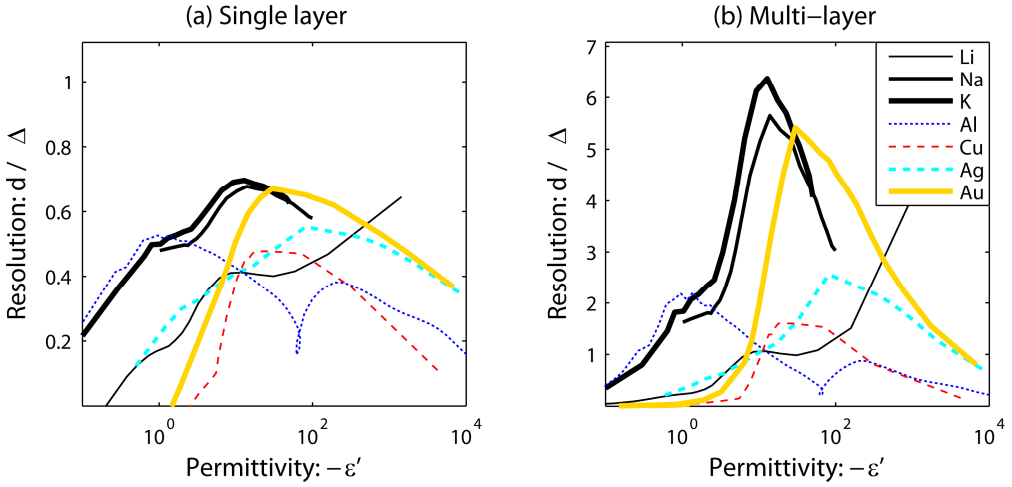

Fig. 4. Thickness:resolution ratio for (a) single and (b) multilayer planar plasmonic lenses (higher is better). Note that since the operating condition is independent of geometry, scaling for background consists of choosing a particular value of the independent variable.

As is well known, enhanced resolution is predicted for multilayer compared to single layer lenses, but note the increased difficulty of constructing multilayer lenses and the potential for the introduction of prohibitive damping due to structural imperfections [37]. Overall the ranking of metals is the same between the two cases. It is clear that for air-embedded lenses, potassium, sodium and aluminium perform much better, but note that only the wavelength for potassium is readily available and it is very reactive. The case for silver, which is commonly used, improves significantly with increased index, and gold would match the alkalis if a sufficiently strong dielectric were available. Maximum performance for most

#106659 - $15.00 USD Received 21 Jan 2009; revised 23 Feb 2009; accepted 24 Feb 2009; published 26 Feb 2009

metals would be achieved for background permittivities greater than silicon and thus cannot be accessed in practice.

It is important to note that these expressions have limits on their validity, especially the single layer case, and that a fuller treatment of imaging produces more complicated results [38]. In particular, the SPP resonance itself is antagonistic to the imaging of arbitrary objects, which is apparent when there is insufficient damping due to very thin films or very low ε''. Additionally, the mathematics of the approximations require that the damping is not too large, so films must be thinner than the excitation wavelength and $\varepsilon'' << \left|-\varepsilon'\right|$. In practice, these constraints are often satisfied and thus the equations provide a reasonable indication of performance. Generally, the approximations leading to Eq. (11) are much less robust than those of Eq. (12), and there are significant differences in the actual transmission near cutoff. Further, when compared to the same cutoff as the single-layer lens ($|t| = 1/2$), the multilayer case is $\cosh^{-1}(2) \approx 1.3$ times better than suggested by Eq. (12). On the other hand, a finite number of layers degrades performance compared to Eq. (12) and electron-confinement effects are presumably increased as the number of layers increases.

It is tempting to try to link the resolving power to actual absorption in the lens, for example by considering energy transport in a plane wave expansion and assuming a non-perturbing imaging layer, absorption of evanescent waves can be shown to be proportional to the imaginary part of the reflection coefficient r:

$$A \propto \begin{cases} 1-|r|^2-|t|^2 & : k_t < k \\ 2\Im\{r\} & : k_t > k \end{cases}, \tag{13}$$

where k_t is the transverse wavevector. For propagating waves this is easily related to the absorptance, but for evanescent waves there is no agreed way to normalise it. In the case of the multilayer lens Eq. (13) essentially complements transmission indicating a positive association with limited resolution. Single layer lenses have a more complicated relationship between transmission and absorption, but there is a qualitative link between metal permittivity and overall absorption, and relative dominance of absorption over transmission beyond cutoff. However, it is probably wise not to infer too much from these observations because it is difficult to separate the effect of coupling at the interfaces, and for example non-absorbing permittivity deviations also limit resolution.

4. Plasmonic waveguiding

Plasmonic waveguides are a potential candidate for optical computers due to simpler construction than photonic crystals, however, loss should be considered because the maximum transmission length is usually on the order of a millimeter, which is similar to the size of current electronic processing units [1].

Several metrics for plasmonic waveguides have been proposed and analyzed for some materials and planar geometries [39-42]. These include the propagation distance, the mode confinement, and other related quantities such as the quality factor, group velocity, and distance from the light line. We will focus on propagation distance since this is directly related to loss. The mode confinement is also considered an important parameter because it affects coupling distances. Note that there is a fundamental competition between confinement and propagation distance because stronger confinement increases metal absorption. The group velocity is important in terms of dispersion engineering and there is presently a lot of interest in slow light in general. We will not consider this in detail, but it is worth noting that group velocity is slow or even negative at high spatial frequency but this is usually accompanied by strong damping; hence we will focus on the low frequency region where a range of positive group velocities are seen. In this regime energy flow can be approximately

#106659 - $15.00 USD Received 21 Jan 2009; revised 23 Feb 2009; accepted 24 Feb 2009; published 26 Feb 2009

related to group velocity, but not necessarily rigorously so in general [43]. In fact, careful analysis shows that energy usually flows in opposite directions on either side of a plasmonic interface, note also that maximum spatial frequency is limited by metal losses. Some investigations of quality factors have been made [39, 44], but given the absence of a simple expressions for the general case we will not consider these further.

The first step in determining guiding parameters is to calculate the dispersion relationship of the complex wavevector parallel to the surface $k_t = k' + ik''$ at a given frequency ω. This is then used to derive metrics such as the absolute propagation length given by $L = 1/(2k'')$. We will investigate the ratio k'/k'' since it is dimensionless. A number of shapes have been proposed for such waveguides [39, 44-46], but we focus on the simplest consisting of flat slabs of metal [8, 47] to gain insight into some of the essential physics. The dispersion relationship for a SPP at a single metal-dielectric interface can be expressed in closed form. Essentially it predicts two operating regions divided by the point $k' \sim \omega\sqrt{\varepsilon_b/2}/c$: the low frequency side where the SPP has dispersion only slightly outside that of free-propagation, and higher frequencies with permittivities $\varepsilon' \to -\varepsilon_b$ that have very low group velocity. Given the simplicity of this solution it is not surprising various aspects have been covered extensively [8, 41]. In particular, the complex wavevector parallel to the surface can be approximated for the low loss case as:

$$k_t \approx \frac{\omega}{c}\left[\frac{\varepsilon'\varepsilon_b}{\varepsilon'+\varepsilon_b}\right]^{1/2}\left[1+i\frac{\varepsilon''\varepsilon_b}{2\varepsilon'(\varepsilon'+\varepsilon_b)}\right] \tag{15}$$

This approximation, as shown in Fig. 5(a), works reasonably well for good metals when $k' << \omega\sqrt{\varepsilon_b}/c$, but it is not generally accurate at high spatial frequencies.

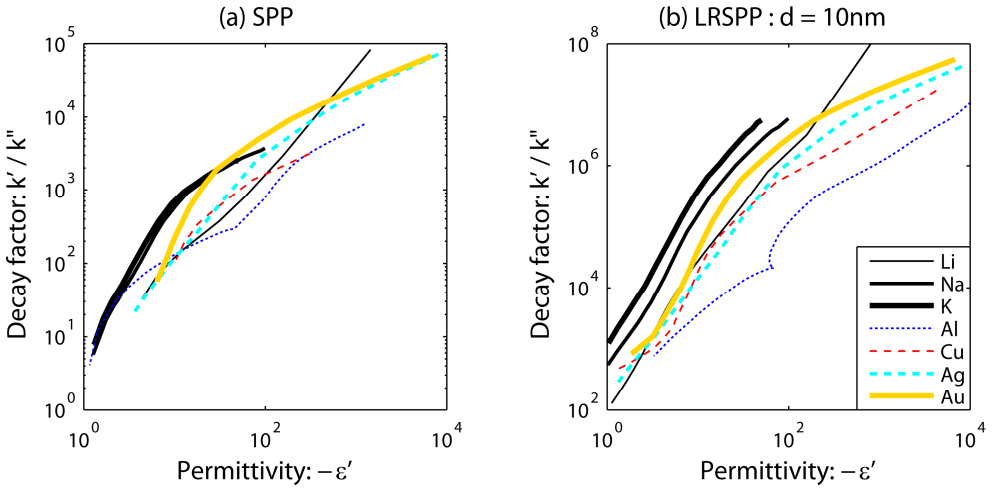

Fig. 5. Approximate decay quality of high frequency modes, from single-interface SPP (a) using Eq. (15) and long-range film plasmon using Eq. 2 from [44] (b).

Practical systems must be limited in thickness, the most obvious solution consisting of a film of metal. The presence of two guides (the interfaces) results in a coupled system that has two bound modes that can be identified on the basis of their frequency and symmetry. The higher frequency mode is less strongly confined and therefore of longer range (LRSPP). A closed-form approximation for thin films at low frequencies is given by Bozhevolnyi and Søndergaard (Eq. 2 in [44]), which is shown in Fig. 5(b). Assuming very thin films and that frequency is not too low, this expression may be further reduced to:

#106659 - $15.00 USD Received 21 Jan 2009; revised 23 Feb 2009; accepted 24 Feb 2009; published 26 Feb 2009

$$k_t \to \frac{\omega}{c}\sqrt{\varepsilon_b}\left[1+i\varepsilon''\left(\frac{\omega d\varepsilon_b}{2\varepsilon'}\right)^2\right]. \tag{16}$$

Note how this improves with reduced film thickness.

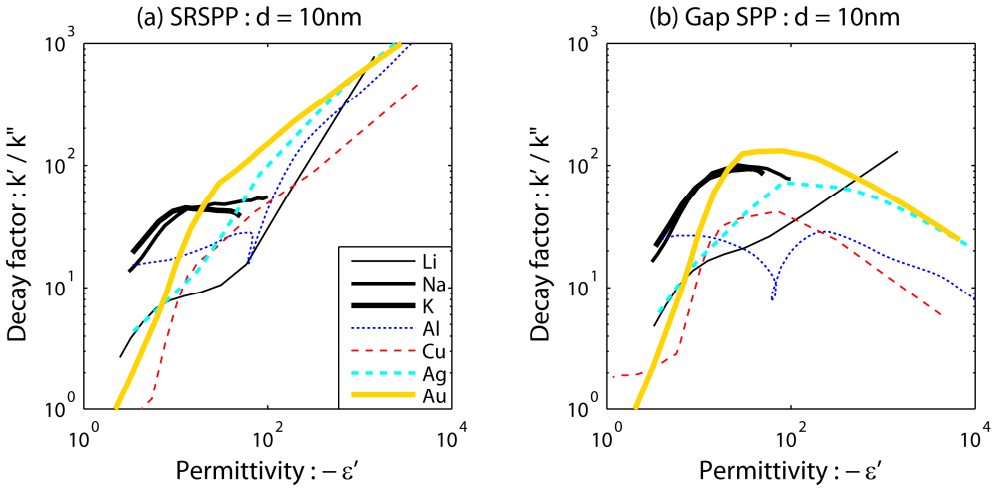

Fig. 6. Approximate decay quality of low frequency short range modes, film short range (a) using Eq. 2 from [44] and gap (b) using Eq. 4 from [44]. Note that due to relatively high real wavevector, the absolute propagation lengths are very low.

The low frequency solution given by Bozhevolnyi and Søndergaard (Eq. 2 in [44]) is strongly confined and short-ranged (SRSPP), as demonstrated in Fig. 6(a), and simplifies to:

$$k_t \to \frac{-2\varepsilon_b\varepsilon'}{d|\varepsilon|^2}\left[1-i\frac{\varepsilon''}{\varepsilon'}\right] \tag{17}$$

The thinner the film the more pronounced the difference between the two modes, and note especially that the single SPP and film LRSPP are adversely affected by increased background permittivity, whereas the short range mode is affected in terms of absolute lengths but not relative to the propagation wavelength.

A less obvious dual guide is the gap between two relatively thick slabs of metal. Aside from a further splitting that must result from additional interfaces, the modes of the gap have different behaviour to those of the film. Importantly, gap and the related channel plasmons [46] can achieve a better compromise between field confinement and propagation length. Equation 4 from the work of Bozhevolnyi and Søndergaard [44] was used in Fig. 6(b), which shows that the gap plasmon has somewhat similar dispersion to the film SRSPP at least for lower permittivities. This equation is more difficult to reduce, but it can be shown empirically that Eq. (17) applies but over a more restricted range of frequencies.

Unfortunately, all of the order-of-magnitude estimates for LR, SR, and gap plasmons require very thin layers, much less than 10nm for 10% error over a reasonable range, which is hard to achieve in practice and would be significantly modified by additional damping processes. Fortunately the error is consistent, so this can be used to select the best metal at a given permittivity. The estimates for the short range plasmons are consistently underestimated, obscuring the actual improvements available at low frequency, whereas the LRSPP estimate is less consistent but the overall trend is preserved. As seen in Fig. 5 & Fig. 6, the single interface and film modes all propagate longer at very negative permittivities, meaning that Al is not particularly competitive overall. The alkali metals perform extremely well for the long range mode due to low plasma frequency, and they also perform well at

#106659 - $15.00 USD Received 21 Jan 2009; revised 23 Feb 2009; accepted 24 Feb 2009; published 26 Feb 2009

moderate permittivity for short-range modes. The gap plasmon peaks at moderate permittivities, and gold gives the longest propagation length in this case.

7. Conclusion

The reason for comparison based on the real part of the permittivity should now be quite clear – together with the background permittivity it determines the operating point of the system. The performance of several systems has been shown to be inversely proportional to the imaginary part of the permittivity, as expected. Importantly, the performance also depends on some power of the real permittivity and some power of the frequency, which both affect the metallic absorption via field enhancement and energy transfer scaling. The frequency does have a significant effect which varies markedly between metrics, so it must be included as part of the dependent variables.

Once the performance as a function of permittivity is determined, in some circumstances it is a simple case of choosing background permittivity and geometric conditions to optimize performance. Choices for background permittivity are relatively limited by the availability of dielectric media, but fortunately some applications allow considerable tuning through geometry. Notable examples of this are the LSP resonances of spherical-shells and nanorods, that can be tuned away from the lossy interband transitions of gold and silver, improving performance from poor to excellent.

It is fair to say that no single metal excels consistently across the board, and the performance achieved can depend significantly on the technical preparation conditions for the metal. In terms of optical properties K & Na appear to be the most consistent, only bettered by Li at high permittivities. The more inert metals are more physically robust – Al optically performing very well at low permittivities and Ag & Au at high permittivities. The limited performance and also limited choice of excitation frequencies leaves considerable scope for improvement, perhaps by band-engineering of metallic compounds [10].

Acknowledgments

We acknowledge useful discussions with Mike Ford, Michael Cortie, Nikolai Zheludev and Kevin MacDonald, and the computational resources of APAC & AC3. We acknowledge financial support from UTS (MA) and the Australian Research Council (MB).

#106659 - $15.00 USD Received 21 Jan 2009; revised 23 Feb 2009; accepted 24 Feb 2009; published 26 Feb 2009